

Wind-Mixed Layer Deepening Scaling Law in a Rotating Frame

M. Coppin¹, B. Deremble¹, J. Sommeria²

¹IGE, CNRS UMR5001, Grenoble, France

²LEGI, CNRS UMR5519, Grenoble, France

Key Points:

- We set a theory for a scaling law of the deepening of the mixed layer induced by the wind forcing
- We show the vertical inhomogeneity of the mixing efficiency within the mixed layer

Corresponding author: Max Coppin, max.coppin@univ-grenoble-alpes.fr

Abstract

The deepening of the mixed layer (ML) is a phenomenon forced by wind stress or heat flux. Scaling laws exist to predict its evolution but they either do not take into account the Earth's rotation or do not explain the turbulent mixing mechanisms involved. Here, we study the case of the formation of a wind-mixed layer in a linearly stratified and rotating ocean. We describe the turbulent mixing processes in an analytical framework using the $k-\epsilon$ model. We show that mixing is mainly confined to a marginally stable interface layer at the bottom of the ML. We also propose a scaling law for the time dependence of the deepening rate of the ML $h \sim t^{1/5}$ as a function of the mixing efficiency the potential energy conversion and the dissipation profile.

Keyword: Mixed-layer depth, Mixing-efficiency, TKE, Turbulent convection, Sear-driven turbulence

Plain Language Summary

1 Introduction

The Mixed layer depth (MLD) deepening is characterised by turbulent convective mixing caused by mechanical stress (momentum flux) or by a change in buoyancy (heat flux). Its dynamics is also affected by the Earth's rotation. The coriolis parameter plays a stabilising role by reducing turbulent convection mixing (Jones and Marshall (1993); Sander et al. (1995); Mironov et al. (2000)), reducing convective instability (Veronis (1959); Chandrasekhar (1997); Carpenter et al. (2022)) and reducing its velocity (Fernando et al. (1991)).

Pollard et al. (1973) (hereafter P73) studied the evolution of the mixing layer (ML) for a constant surface stress with no heat fluxes and constant stratification. They established a scaling law used in a large number of models (Zilitinkevich et al. (1979), Lozovatsky et al. (2005)). It is particularly robust in a stationary reference frame (Ushijima and Yoshikawa (2020)), but their scaling is only valid for one inertial period. For longer time, Pollard et al. (1973) proposed that the ML reaches a maximum and no longer deepens. However, it appears that there is a change in the regime at half of the inertial period and the mixing layer continues to deepen (Ushijima and Yoshikawa (2020)). They studied the evolution of h in the rotational case and obtained a law $h(t) \sim t^{0.18}$ using LES simulations. However, they did not provide the mechanisms that could explain this scaling law.

P73 formalize a scaling law for the depth of the mixed layer h forced by a constant wind stress τ , in a linear ambient stratification N . It is a separated expression for time inferior and superior of half the inertial time scale $T_f = 2\pi/f$

$$h(t) = \left(\frac{\tau}{\rho}\right)^{1/2} \left[\frac{4(1 - \cos(ft))}{f^2 N^2} \right]^{1/4} \quad t < \pi/f \quad (1)$$

$$= 1.7 \left(\frac{u_*}{\sqrt{Nf}} \right) \quad t > \pi/f \quad (2)$$

with $u_* = \sqrt{\frac{\tau}{\rho}}$ the friction velocity at the surface and we use the notation

$$L_{P73} = \frac{u_*}{\sqrt{Nf}} \quad (3)$$

as characteristic length from the P73's scaling law.

We also define from the equation (3.1) in the paper of P73 a characteristic velocity of the ML U_{p73}

$$U_{p73} = \frac{u_*^2}{f L_{p73}}. \quad (4)$$

Ushijima and Yoshikawa (2020) (hereafter U20) used LES numerical model to propose a time-dependant scaling of the ML depending on the Rossby number and the Froude number that can be extended further the inertial period

$$h = 1.5L_{p73} \left(\frac{f}{N} \right)^{-2.2 \times 10^{-2}} \left(\frac{t}{T_f} \right)^{0.18}. \quad (5)$$

In this paper we are interested in the physical process involved in the ML formation after the half of an inertial period. We propose to diagnose the ML deepening mechanism in presence of rotation by using idealised 1D numerical simulations. Then to build a theoretical frame for a scaling law. We begin in section 2 by describing the $k-\epsilon$ turbulent closure model. In section 3 we quantify the energy exchanges in the water column. A diagnostic of mixing and dissipation is given in section 4. In section 5 we formalise the scaling law and explore the limits of the proposed assumption. We conclude in section 6.

2 Model and Methods

2.1 $k - \epsilon$ Model

The $k - \epsilon$ model is a turbulent closure of order 2. It closes the Reynolds's average equation by adding two prognostic transport equations, one for the turbulent kinetic energy k and the other for the dissipation ϵ . Neglecting advecting terms.

$$\frac{\partial k}{\partial t} - \frac{\partial}{\partial z} \left(\left(\nu + \frac{\nu_t}{\sigma_k} \right) \frac{\partial k}{\partial z} \right) = P - B - \epsilon \quad (6)$$

$$\frac{\partial \epsilon}{\partial t} - \frac{\partial}{\partial z} \left(\left(\nu + \frac{\nu_t}{\sigma_\epsilon} \right) \frac{\partial \epsilon}{\partial z} \right) = \frac{\epsilon}{k} (c_{1\epsilon} P - c_{3\epsilon} B - c_{2\epsilon} \epsilon) \quad (7)$$

Where σ_k the turbulent Schmidt number, $c_{1\epsilon}, c_{2\epsilon}, c_{3\epsilon}$ empirical parameters (Canuto et al. (2001)).

The turbulent fluxes are computed as follows Rodi (1987) Burchard (2002b)

$$P = -\overline{u'w'} \partial_z \bar{u} = \nu_t (\partial_z \bar{u})^2 \quad (8)$$

$$B = \overline{w'b'} = -\nu'_t (\partial_z \bar{b}) \quad (9)$$

with $b = -g \frac{\Delta \rho}{\rho}$ and the diffusivity ν_t and ν'_t respectively of momentum and heat are parameterised using stability functions c_μ and c'_μ (Canuto et al. (2001); Burchard and Bolding (2001)) such that :

$$\nu_t = c_\mu \frac{k^2}{\epsilon} \quad \nu'_t = c'_\mu \frac{k^2}{\epsilon} \quad (10)$$

This model has been shown to be robust in convective processes (Burchard and Bolding (2001); Umlauf et al. (2003)) since it correctly reproduces the basic interaction mechanisms between shear, stratification and turbulence. This model is well adapted to our study since it contains no a priori assumptions about the structure of the water column. A cross-sectional study of turbulence closure models, and in particular the $k-\epsilon$ model, is presented in (Burchard, 2002a).

2.2 Numerical Model

We use the open-source numerical model GOTM (General Ocean Turbulence Model) <https://gotm.net/>. This Model solves the momentum, salt and heat transport equations over a 1D water column. All horizontal gradients are either parameterised, neglected,

81 or obtained prognostically where possible. Our configuration solves equation (7) for a
 82 Coriolis parameter $f \in [0; 1.45 \cdot 10^{-4}] \text{ s}^{-1}$, a stratification $N^2 \in [10^{-6}; 10^{-3}] \text{ s}^{-1}$ and
 83 a forcing $\tau_x = 1.10^{-1}$, a simulation span of 10 j for a time step of 60 s. The vertical
 84 resolution is 50 cm for a domain of 500 m in the z -axis.

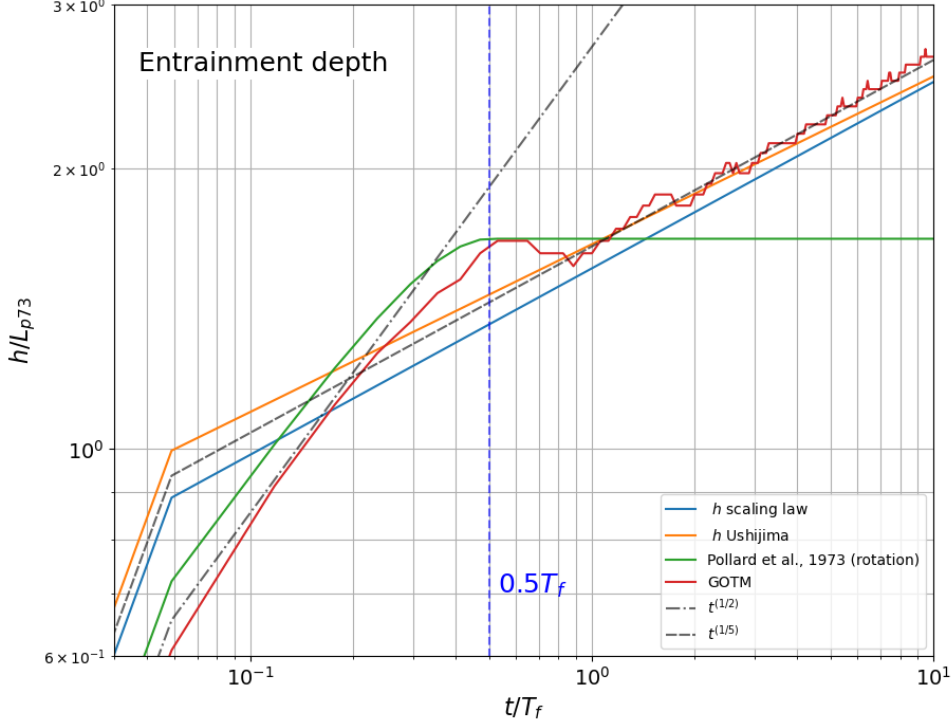


Figure 1. Time evolution of the mixed layer depth (MLD) in solid lines simulated by the numerical model (red), the scaling law predicted by Pollard et al (green), the scaling law found by U20 (in orange) and the analytical scaling law demonstrated in this paper (in light blue). Dark dashed line are the temporal evolution power 1/2 and 1/5. The vertical dashed blue line indicates half of the inertial period $0.5T_f$. The Coriolis parameter for the analytical law and the simulation is $f = 10^{-4} \text{ s}^{-1}$, $N^2 = 10^{-4} \text{ s}^{-1}$ and the wind stress $\tau = 0.1027 \text{ m}^2 \text{ s}^{-2}$

85 Figure 1 show the evolution of h in time using this model, we retrieve an evolution
 86 law $h(t) \sim t^{1/5}$ which is near the value found by U20 $h_{U20}(t) \sim t^{0.18}$. This numerical
 87 model does well reproduce the ML deepening and thus comfort our model choice.

3 Energetic of the Mixed Layer Deepening

3.1 Potential Energy Evolution

The deepening process is a modification of the background density profile

$$\rho_i(z) = \rho_0 \left(1 - \frac{N^2}{g} z \right)$$

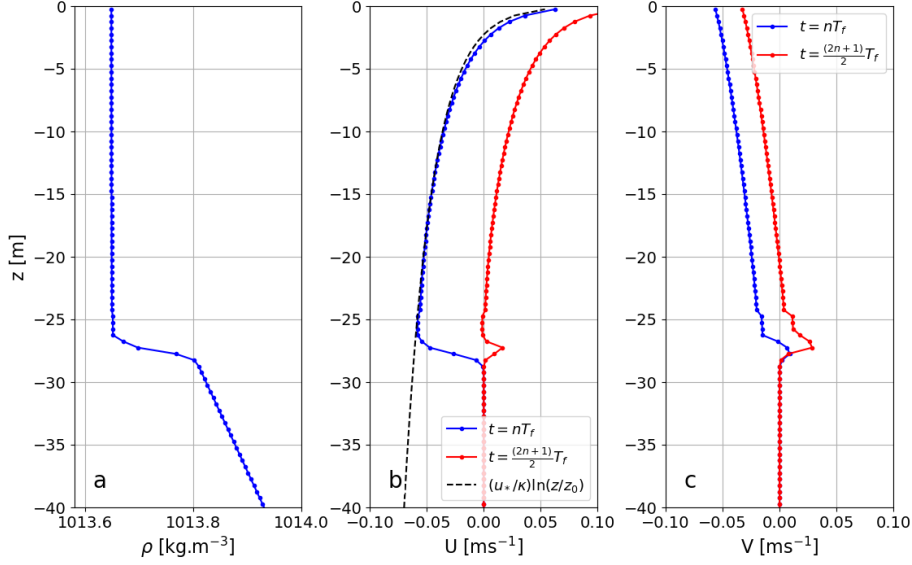


Figure 2. Vertical profile of (a) density, (b) along-wind velocity U and (c) cross-wind velocity V . In blue, the last inertial period $t = 13 T_f$. In red the last half inertial period $t = 12.5 T_f$. In black the logarithmic profile of the velocity from the "Law of the wall" $\frac{u_*}{\kappa} \ln(z)$. The parameters of the simulation are : $f = 10^{-4} \text{ s}^{-1}$, $N^2 = 10^{-4} \text{ s}^{-1}$ and the wind stress $\tau = 0.1027 \text{ m}^2 \text{ s}^{-2}$

into a homogeneous density ρ_m By making the assumption of a linear stratification

$$\rho_m = \frac{\rho_i(z=0) + \rho_i(z=-h)}{2} = \rho_0 \left(1 - \frac{N^2}{2g} h\right). \quad (11)$$

As h deepens, the density ρ_m of the mixing layer increases because it has been mixed with the denser water below. Therefore, over time, the centre of mass of the ML is shifted upward. Considering a vertical density profile of a water column composed by a mixed layer and a stratified one, we can write the expression of the potential energy in two parts, one for each layer.

$$\begin{aligned} E_p &= \overbrace{\int_{-h}^0 \rho_0 \left(1 - \frac{N^2}{2g} h\right) g z dz}^{E_p^m} + \overbrace{\int_{-H}^{-h} \rho_0 \left(1 - \frac{N^2}{g} z\right) g z dz}^{E_p^{strat}} \\ &= \rho_0 \left(-\frac{gH^2}{2} - \frac{N^2 H^3}{3} + \frac{1}{12} N^2 h^3 \right) \end{aligned}$$

The first two terms correspond to the background potential energy and the last term represent the gain due to the lift of the centre of mass. Taking the derivative of this equation gives the time evolution of the potential energy, which is positive. Thus, a deepening of the mixed layer is correlated to gain of potential energy. For the rest we adimensionalize the energy by the density.

$$\frac{dE_p}{dt} = \frac{N^2}{12} \frac{dh^3}{dt} \quad (12)$$

3.2 Buoyancy Production

We consider the Buoyancy equation in the Boussinesq approximation using the $k-\epsilon$ model for the heat turbulent diffusivity $\nu'_t = c'_\mu \frac{k^2}{\epsilon} = \frac{\nu_t}{Pr}$. Where c'_μ is a stability function ((“Idealised test cases”, 2002)), k the turbulent kinetic energy and ϵ the dissipation, Pr the Prandtl number.

$$\frac{\partial b}{\partial t} - \frac{\partial}{\partial z} \left(\nu'_t \frac{\partial b}{\partial z} \right) = 0 \quad (13)$$

Setting $e_p = -zb$ we can rewrite (13) into the potential energy equation by multiplying by $(-z)$ and integrating by part.

$$\frac{\partial e_p}{\partial t} - \frac{\partial}{\partial z} \left((-z) \nu'_t \frac{\partial b}{\partial z} \right) = \nu'_t \frac{\partial b}{\partial z} \quad (14)$$

Since the value of the thermal turbulent diffusivity at the bottom is null the integration of the equation (14) over the column gives

$$\frac{\partial E_p}{\partial t} = \int_{-H}^0 \nu'_t \frac{\partial b}{\partial z} dz = \int_{-H}^0 -B dz. \quad (15)$$

Here the capital E_p refer to the integrated potential energy e_p and B refer to the Buoyancy production. This balance show the production of buoyancy is equal to the evolution of the potential energy. That means the change of the MLD, using the eq (12) above, can be directly describes by the turbulent buoyancy production.

3.3 Local Turbulent Kinetic Energy Balance

The input of energy at the top of the water column is converted into turbulent Shear, which is transported in the water column by turbulent processes. The evolution of the MLD can be retrieved by the buoyancy production. We thus need to consider the turbulent kinetic energy (k) equation (7).

At first, as the near sub surface velocity increase, accelerating the mixed layer. After half of the inertial period we see in Fig 3 (Top) that the velocity drops due to the onset of an inertial oscillation. As a result the layer reaches a periodic equilibrium. However there is still an injection of energy at the surface and the mixing layer continues to deepen as the fig 1 shows but does not accelerate. As a result we observe TKE reaching steady as shown Fig (3) (Bottom)

Thus there is a balance between the terms on the right hand sides.
Hence

$$P - B = \epsilon. \quad (16)$$

We can use the expression of the Richardson flux $Ri_f = \frac{-B}{P}$ in the equation (16)

$$1 + \frac{P}{B} = -\frac{\epsilon}{B} \quad (17)$$

$$-B = \frac{Ri_f}{1 + Ri_f} \epsilon \quad (18)$$

$$-B = \Gamma \epsilon \quad (19)$$

With the mixing efficiency $\Gamma = \frac{Ri_f}{1 + Ri_f}$. This equation is a relationship between the production of buoyancy, dissipation and mixing efficiency. We have also considered this equilibrium from a local point of view.

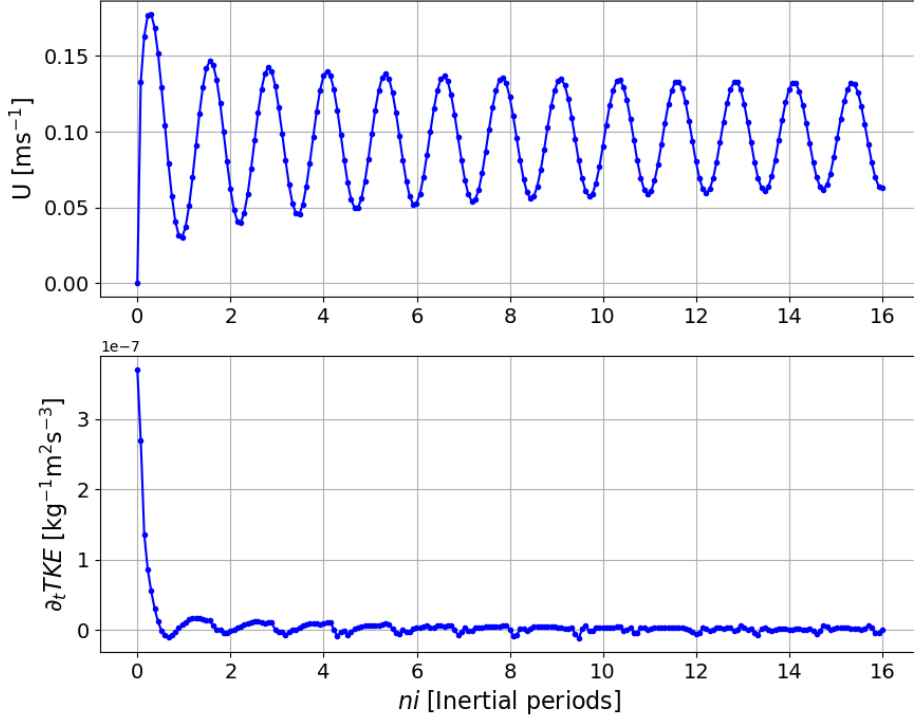


Figure 3. Time evolution of the time derivative of the surface along-wind velocity (Top) and TKE integrated over the water column (Bottom). $f = 10^{-4} \text{ s}^{-1}$, $N^2 = 10^{-4} \text{ s}^{-1}$ and the wind stress $\tau = 0.1027 \text{ m}^2 \text{ s}^{-2}$

Although we consider a mixing layer, nothing suggests that the mixing process is uniform in this layer. The subject of the next section is, therefore, the nature of the mixing and dissipation and their vertical distribution.

4 Mixing and Dissipation law

4.1 Interface Mixed/Stratified layer

If we consider the water column during the deepening process of the mixed layer in a case forced by the surface shear, we can consider three parts. The first is the mixed layer. With $z \in [0, -h+h_i]$ In this layer, the velocity has a logarithmic profile and given that the layer is already mixed and therefore homogeneous, we can assume there is very little mixing. The second part $z \in [-h+h_i, -h]$ which we call the "interface layer" of thickness h_i contains the density jump between the other two parts. It is therefore in this layer that the mixing is greatest. This mixing is caused by a velocity shear which is all the greater the thinner its thickness. This layer is therefore marginally stable which means its Richardson number takes a critical value. Then the bottom layer. With $z \in [-h, -H]$. This layer is not affected by the surface shear and is therefore at rest with the background stratification and so zero mixing. The second part is the mixed layer. With $z \in [0, -h+h_i]$ In this layer, the velocity has a logarithmic profile and given that the layer is already mixed and therefore homogeneous, we can assume there is very little mix-

ing.

$$Ri = \frac{g \frac{\partial \rho}{\partial z}}{(\frac{\partial U}{\partial z})^2} = Ri_c \quad (20)$$

with the density leap: $\frac{\partial \rho}{\partial z} = \frac{N^2 h}{h_i}$

We observe in Fig (3 (b)), that the velocity in the ML follow a logarithmic profile

$$\frac{\partial \bar{u}}{\partial z} = \frac{u_*}{\kappa z} \quad (21)$$

with κ the Von Karman constant. This expression com from the *law of the wall* due to the frictional behaviour of the wind stress. We also see that the velocity profile is oscillating between a peak and a trough of the inertial period. As a result, the shear at the bottom of the mixing layer varies within an inertial period. The first consequence of this is that we need to estimate an average value for this shear between $-h + h_i$ and $-h$. We use the characteristic velocity U_{p73} (4). Furthermore, in order to obtain a power law, we need to make a logarithmic correction. We therefore obtain an expression for the velocity shear between the mixed layer and the stratified layer at rest

$$\frac{\partial U}{\partial z} = \frac{u(-h + h_i) - 0}{h_i} = \frac{u_* \sqrt{\frac{N}{f}}}{h_i}. \quad (22)$$

The second consequence is that the marginal stability condition is also periodic since it is only valid for a sufficiently large shear. The precise evaluation of the Richardson number under these conditions is complex, so we will adopt a bulk formulation in the interface layer with $Ri_c = O(1)$. This formulation is commonly used in ML deepening models (Pollard et al. (1973); Price et al. (1986)).

Hence, we obtain a relation for the interface layer thickness

$$h_i = Ri_c \frac{u_*^2}{N f} \frac{1}{h} \quad (23)$$

4.2 Mixing efficiency

As we have seen, mixing is negligible throughout the water column except in the interface layer. Moreover, mixing efficiency is often defined empirically ((Osborn, 1980)) with a value of $\Gamma_{t0} = 0.2$. We therefore approach the Γ profile as a piece-wise constant function taking the value Γ_0 in the interface layer and 0 elsewhere. Fig 4 represent its vertical profile. Our optimal value Γ_0 to fit the numerical values is slightly greater, $\Gamma_0 = 0.3$. This does not affect our scaling since it remains about the same order. From now we will use the approximated function instead of the real profile. We call it Γ for more simplicity.

The integral of the combination of the eq (15) and (19) can be decomposed on the three intervals describe above. Due to the zero value of the mixing efficiency in the mixing layer and the deep layer, we can therefore write

$$\frac{\partial E_{pot}}{\partial t} = \int_{-h}^{-h+h_i} \Gamma \epsilon dz. \quad (24)$$

Now $h_i \ll h$, so we can take the value of ϵ in $z = -h$ discretely and take it out of the integral

$$\frac{\partial E_{pot}}{\partial t} = \Gamma_0 h_i \epsilon(z = -h) = Ri_c \Gamma_0 \frac{u_*^2}{N f} \frac{1}{h} \epsilon(z = -h). \quad (25)$$

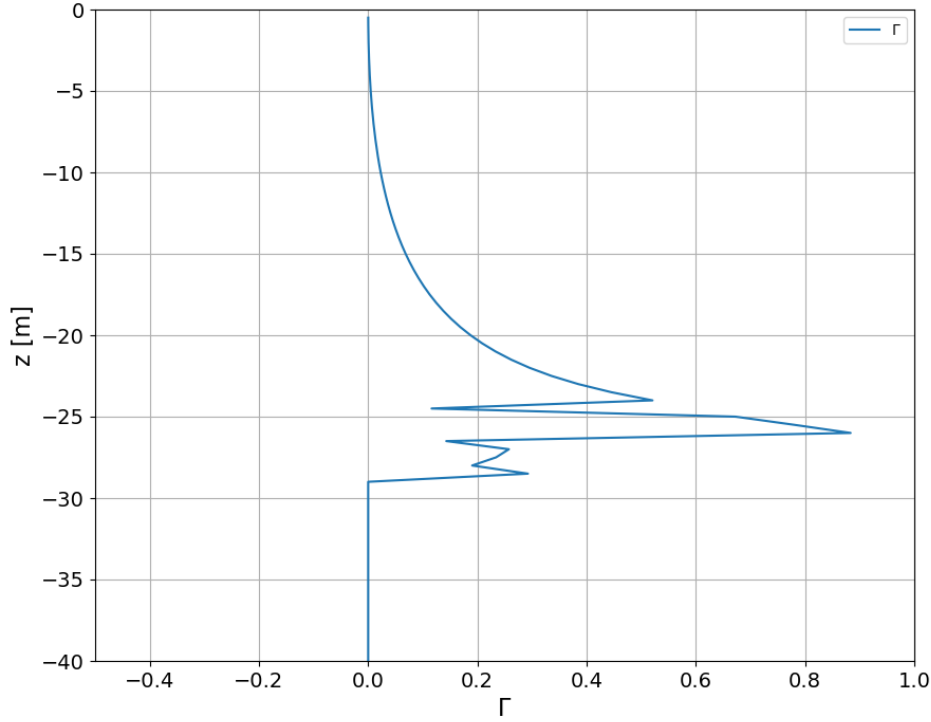


Figure 4. Vertical profile of the mixing efficiency at the last moment of the simulation. The bold line is the profile obtained by the simulations. Implicitly, the contour of the function delimits the three parts: from top to bottom: the Mixed layer, the interface layer and the bottom layer. $f = 10^{-4} \text{ s}^{-1}$, $N^2 = 10^{-4} \text{ s}^{-1}$ and the wind stress $\tau = 0.1027 \text{ m}^2 \text{ s}^{-2}$

4.3 Dissipation Vertical Profile

To determine the nature of the vertical profile of the ϵ dissipation we consider the TKE balance equation. At the surface we have $B = 0$. And as our system is quasi-stationary we have that $\frac{\partial k}{\partial t} = 0$. Hence, near the surface

$$\epsilon = -P.$$

The vertical profile of the dissipation is assumed by interpolating its surface expression throughout the mixed layer. Using the logarithmic profile of the velocity (Fig 21) and using the constant flux approximation $u'w' = u_*^2$

$$\epsilon(z) = \frac{u_*^3}{\kappa z} \quad (26)$$

The approximation we made by interpolating the surface dissipation expression over the entire mixing layer is quite good, since we observe in Fig (5) the same order of magnitude at the top of the interface layer, (above the leap).

Using the equations (12),(25)

$$\frac{N^2}{12} \frac{\partial h^3}{\partial t} = Ri_c \Gamma_0 \frac{u_*^2}{Nf} \frac{1}{h} \epsilon(z = -h) \quad (27)$$

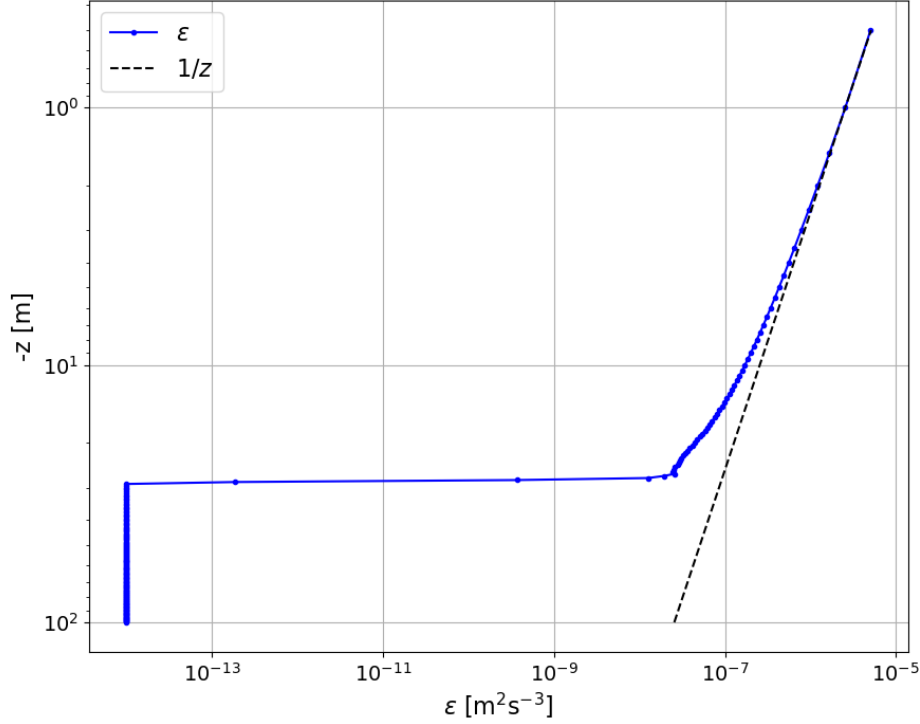


Figure 5. Vertical profile of the dissipation ϵ (blue solid line) the last instant of the simulation. And a law $1/z$ (dashed line). T. $f = 10^{-4} \text{ s}^{-1}$, $N^2 = 10^{-4} \text{ s}^{-1}$ and the wind stress $\tau = 0.1027 \text{ m}^2 \text{ s}^{-2}$

192 and by replacing the expressions of the dissipation at the depth h using 26

$$\frac{\partial h^5}{\partial t} = \left(20 Ri_c \Gamma_0 \frac{u_*^5}{N^3 f \kappa} \right) \quad (28)$$

193 and by time integration

$$h(t) = \left(20 Ri_c \Gamma_0 \frac{u_*^5}{N^3 f \kappa} \right)^{1/5} t^{1/5}. \quad (29)$$

194 We write this equation using the same formulation as Ushijima and Yoshikawa (2020)

$$h(t) = L_{p73} \left(40 \pi Ri_c \frac{\Gamma_0}{\kappa} \right)^{1/5} \left(\frac{f}{N} \right)^{1/10} \left(\frac{t}{T_f} \right)^{1/5} \quad (30)$$

195 We therefore obtain a law that predicts deepening at a rate $t^{1/5}$. This rate is consistent
 196 with the one computed by U20. We also note that the coefficient $\frac{f}{N}$ is quite different
 197 from the value of U20 but remain very small and the sensibility of the scaling law
 198 within the range of the $(\frac{f}{N})$ values set by U20 ($\frac{f}{N} = 1.3 \times 10^{-3}$ for the smallest and
 199 $\frac{f}{N} = 2.0 \times 10^{-4}$ for the greatest) is negligible. We can compare in Fig (1) the value

of our scaling (S) to the value obtain with the scaling of U20 and the numerical simulation. We observe our scaling underestimate the ML deepening. However, because the time dependency is greater in our formulation than the U20 one. The relative error of our MLD estimate to U20 $\frac{h_{U20} - h_s}{h_{U20}}$ reduce from 4.5 % to 2 % to 1 % to 12 % T_f . We do not consider longer times because then we would exceed the time scale of a constant surface wind and we would have to consider other processes. We can therefore conclude to the constancy of our scaling law and show the validity of our theoretical framework.

4.4 Limitations

In this study we have made a number of approximations and assumptions. We have considered each of these to be valid as long as they respect the same order of magnitude as the simulated values. We summarise them here:

- We wanted an analytical solution in the form of a power law of the deepening rate of the ML. Thus we had to consider the stratification to be linear and apply logarithmic corrections to the velocity at the base of the interface layer.
- We approximated the mixing efficiency profile to be non-null only in the interface layer. In reality, mixing is still occurring in the upper part of the ML since its density increases as the layer thickens, as shown by its expression eq (11). In the deep layer below the ML, internal waves are generated by the deepening of the ML, creating some mixing.
- We interpolated the dissipation profile from a valid surface expression.
- We have used the expression of a critical Richardson number to define the thickness of the interface layer. This approach is more refined than a Bulk Richardson number over the entire ML (Pollard et al. (1973); Price et al. (1986)). Yet, due to inertial oscillations, this layer is in a marginal stability state only when the shear at the base of the ML is maximal.

5 Concluding Remarks

In this study we have developed a theoretical framework to explain the deepening of the ML in the case of an ocean forced by surface stress without heat loss in a rotating frame. The deepening rate was found to be function of the Coriolis parameter and the stratification with the time dependency $h(t) \sim t^{1/5}$. We have showed that the turbulent kinetic energy reach a steady state after 0.5 T_f . Thus the constant input of energy by wind stress on the surface is converted to buoyancy production in a layer at the interface between the well-mixed layer above and the stratified one at rest below. This interface is defined by its marginal stability and concentrate most of the mixing. Therefore we shown the vertical inhomogeneity of the mixing efficiency within the mixed layer.

All the processes are studied in 1D in the classical framework referred by Taylor and Ferrari (2010) as "upright convection" and therefore does not take into account horizontal density gradients. In their paper, Taylor and Ferrari (2010) showed that considering a baroclinic fluid referred as "slantwise convection" led to a different convection from the point of view of the PV structure and which had a different dynamical regime. It would therefore be interesting to extend this work on the diagnosis of 3D mixing processes to a baroclinic fluid.

Acknowledgments

This work has been funded by the IRGA grant 2023, distributed for the laboratory from the university of Grenoble Alpes, and the grant ANR PLUME. The authors declare that they have no conflict of interest.

References

- Burchard, H. (2002a). *Applied Turbulence Modelling in Marine Waters*. Springer Science & Business Media.
- Burchard, H. (2002b). Energy-conserving discretisation of turbulent shear and buoyancy production. *Ocean Modelling*, 4(3), 347–361. doi: 10.1016/S1463-5003(02)00009-4
- Burchard, H., & Bolding, K. (2001). Comparative Analysis of Four Second-Moment Turbulence Closure Models for the Oceanic Mixed Layer. *Journal of Physical Oceanography*, 31(8), 1943–1968. doi: 10.1175/1520-0485(2001)031<1943:CAOFSM>2.0.CO;2
- Canuto, V. M., Howard, A., Cheng, Y., & Dubovikov, M. S. (2001). Ocean Turbulence. Part I: One-Point Closure Model—Momentum and Heat Vertical Diffusivities. *Journal of Physical Oceanography*, 31(6), 1413–1426. doi: 10.1175/1520-0485(2001)031<1413:OTPIOP>2.0.CO;2
- Carpenter, J. R., Liang, Y., Timmermans, M.-L., & Heifetz, E. (2022). Physical mechanisms of the linear stabilization of convection by rotation. *Physical Review Fluids*, 7(8), 083501. doi: 10.1103/PhysRevFluids.7.083501
- Chandrasekhar, S. (1997). The instability of a layer of fluid heated below and subject to Coriolis forces. *Proceedings of the Royal Society of London. Series A. Mathematical and Physical Sciences*, 217(1130), 306–327. doi: 10.1098/rspa.1953.0065
- Fernando, H. J. S., Chen, R.-R., & Boyer, D. L. (1991). Effects of rotation on convective turbulence. *Journal of Fluid Mechanics*, 228, 513–547. doi: 10.1017/S002211209100280X
- Idealised test cases. (2002). In H. Burchard (Ed.), *Applied Turbulence Modelling in Marine Waters* (pp. 117–134). Berlin, Heidelberg: Springer. Retrieved 2023-11-02, from https://doi.org/10.1007/3-540-45419-5_6 doi: 10.1007/3-540-45419-5_6
- Jones, H., & Marshall, J. (1993). Convection with Rotation in a Neutral Ocean: A Study of Open-Ocean Deep Convection. *Journal of Physical Oceanography*, 23(6), 1009–1039. doi: 10.1175/1520-0485(1993)023<1009:CWRIAN>2.0.CO;2
- Lozovatsky, I., Figueroa, M., Roget, E., Fernando, H. J. S., & Shapovalov, S. (2005). Observations and scaling of the upper mixed layer in the North Atlantic. *Journal of Geophysical Research: Oceans*, 110(C5). doi: 10.1029/2004JC002708
- Mironov, D. V., Gryanik, V. M., Moeng, C.-H., Olbers, D. J., & Warncke, T. H. (2000). Vertical turbulence structure and second-moment budgets in convection with rotation: A large-eddy simulation study. *Quarterly Journal of the Royal Meteorological Society*, 126(563), 477–515. doi: 10.1002/qj.49712656306
- Osborn, T. R. (1980). Estimates of the Local Rate of Vertical Diffusion from Dissipation Measurements. *Journal of Physical Oceanography*, 10(1), 83–89. doi: 10.1175/1520-0485(1980)010<0083:EOTLRO>2.0.CO;2
- Pollard, R. T., Rhines, P. B., & Thompson, R. O. R. Y. (1973). The deepening of the wind-Mixed layer. *Geophysical Fluid Dynamics*. doi: 10.1080/03091927208236105
- Price, J. F., Weller, R. A., & Pinkel, R. (1986). Diurnal cycling: Observations and models of the upper ocean response to diurnal heating, cooling, and wind mixing. *Journal of Geophysical Research: Oceans*, 91(C7), 8411–8427. doi: 10.1029/JC091iC07p08411
- Rodi, W. (1987). Examples of calculation methods for flow and mixing in stratified fluids. *Journal of Geophysical Research: Oceans*, 92(C5), 5305–5328. doi: 10.1029/JC092iC05p05305
- Sander, J., Wolf-Gladrow, D., & Olbers, D. (1995). Numerical studies of open ocean deep convection. *Journal of Geophysical Research: Oceans*, 100(C10), 20579–20600. doi: 10.1029/95JC02405

- 301 Taylor, J. R., & Ferrari, R. (2010). Buoyancy and Wind-Driven Convection at
 302 Mixed Layer Density Fronts. *Journal of Physical Oceanography*, 40(6), 1222–
 303 1242. doi: 10.1175/2010JPO4365.1
- 304 Umlauf, L., Burchard, H., & Hutter, K. (2003). Extending the k- turbulence model
 305 towards oceanic applications. *Ocean Modelling*, 5(3), 195–218. doi: 10.1016/
 306 S1463-5003(02)00039-2
- 307 Ushijima, Y., & Yoshikawa, Y. (2020). Mixed layer deepening due to wind-induced
 308 shear-driven turbulence and scaling of the deepening rate in the stratified
 309 ocean. *Ocean Dynamics*, 70(4), 505–512. doi: 10.1007/s10236-020-01344-w
- 310 Veronis, G. (1959). Cellular convection with finite amplitude in a rotating fluid.
 311 *Journal of Fluid Mechanics*, 5(3), 401–435. doi: 10.1017/S0022112059000283
- 312 Zilitinkevich, S., Chalikov, D., & Resnyansky, Y. (1979). Modeling the
 313 oceanic upper layer. *Oceanologica Acta*. Retrieved from [https://](https://www.semanticscholar.org/paper/Modeling-the-oceanic-upper-layer-Zilitinkevich-Chalikov/6706329a5065723701d4f194d68adbff12f4cd12)
 314 [www.semanticscholar.org/paper/Modeling-the-oceanic-upper-layer](https://www.semanticscholar.org/paper/Modeling-the-oceanic-upper-layer-Zilitinkevich-Chalikov/6706329a5065723701d4f194d68adbff12f4cd12)
 315 [-Zilitinkevich-Chalikov/6706329a5065723701d4f194d68adbff12f4cd12](https://www.semanticscholar.org/paper/Modeling-the-oceanic-upper-layer-Zilitinkevich-Chalikov/6706329a5065723701d4f194d68adbff12f4cd12)